PAPER

Cellulose nanofibers decorated with magnetic nanoparticles – synthesis, structure and use in magnetized high toughness membranes for a prototype loudspeaker†

Sylvain Galland,[ab] Richard L. Andersson,[a] Michaela Salajková,[ab] Valter Ström,[c] Richard T. Olsson*[ab] and Lars A. Berglund*[ab]

Magnetic nanoparticles are the functional component for magnetic membranes, but they are difficult to disperse and process into tough membranes. Here, cellulose nanofibers are decorated with magnetic ferrite nanoparticles formed *in situ* which ensures a uniform particle distribution, thereby avoiding the traditional mixing stage with the potential risk of particle agglomeration. The attachment of the particles to the nanofibrils is achieved *via* aqueous *in situ* hydrolysis of metal precursors onto the fibrils at temperatures below 100 °C. Metal adsorption and precursor quantification were carried out using Induction Coupled Plasma-Optical Emission Spectroscopy (ICP-OES). FE-SEM was used for high resolution characterization of the decorated nanofibers and hybrid membranes, and TEM was used for nanoparticle size distribution studies. The decorated nanofibers form a hydrocolloid. Large (200 mm diameter) hybrid cellulose/ferrite membranes were prepared by simple filtration and drying of the colloidal suspension. The low-density, flexible and permanently magnetized membranes contain as much as 60 wt% uniformly dispersed nanoparticles (thermogravimetric analysis data). Hysteresis magnetization was measured by a Vibrating Sample Magnetometer; the inorganic phase was characterized by XRD. Membrane mechanical properties were measured in uniaxial tension. An ultrathin prototype loudspeaker was made and its acoustic performance in terms of output sound pressure was characterized. A full spectrum of audible frequencies was resolved.

Introduction

In biological materials, nanostructural control is obtained by bottom-up synthesis procedures. For instance, inorganic nanoparticles nucleate and grow by biomineralization on organic surfaces.[1] This provides the advantage of controlled nanoparticle distribution. In contrast, man-made polymer nanocomposites are often made by simply mixing the nanoparticle and a polymer matrix. Very often, nanoparticles become agglomerated so that macroscopic properties are compromised.[2] We have previously formed magnetic nanoparticles on a bacterial cellulose nanofiber hydrogel scaffold.[3] The hydrogel

was converted to a magnetic aerogel and also to thin films. However, from a processing point of view, it would be interesting to have cellulose nanofibers and ferrite nanoparticles in liquid form. This would allow facile conversion to coatings and membranes by spraying or doctor-blading, in addition to the traditional papermaking processes.

The present study deals with preparation of cellulose nanofibers decorated with magnetic ferrite nanoparticles. The starting material for the nanofibers is cellulosic wood pulp fibers, a low-cost raw material from renewable resources. Cellulose nanofibers combined with ferrite can be envisaged to compete with traditional polymer matrices in highly sophisticated magnetic nanocomposite membranes for purification/filtration and magneto-responsive actuators as well as for the manufacture of anti-counterfeiting papers, radio-frequency materials and flexible data storage.[4,5] A major challenge is to combine the magnetic and mechanical properties at a sufficiently high nanoparticle content (>20 wt%) for applications relying on the magnetic functionality, which would allow significant tuning of the magnetic properties within wide ranges with preserved mechanical performance.[6] The materials typically become brittle due to stress concentration from

[a]*Royal Institute of Technology, School of Chemical Science and Engineering, Department of Fiber and Polymer Technology, Teknikringen 56, 100 44 Stockholm, Sweden. E-mail: rols@kth.se; Fax: +46 73 270 18 68; Tel: +46 8 790 60 36*

[b]*Wallenberg Wood Science Center, Royal Institute of Technology, Teknikringen 56, 100 44 Stockholm, Sweden*

[c]*Royal Institute of Technology, School of Industrial Engineering and Management, Department of Materials Science and Engineering, Brinellvägen 23, 100 44 Stockholm, Sweden*

† Electronic supplementary information (ESI) available: Experimental details, Fig. S1–S7, Table S1, video and audio recordings. See DOI: 10.1039/c3tc31748j

This journal is © The Royal Society of Chemistry 2013

J. Mater. Chem. C, 2013, **1**, 7963–7972 | 7963

magnetic nanoparticle agglomerates, severely limiting their applications.[4,7] Robust and innovative methods for nanoparticle dispersion and stabilization are consequently a key to the development of these new hybrid materials; and inexpensive methods that facilitate implementation on a large scale are desirable.

In this context, natural wood cellulose I nanofibrils (3–5 nm wide and up to a few micrometers in length), the main component of the wood fiber cell wall, can provide a new nanocomposite building block.[8] The fibrils can be isolated by mechanical disintegration[9] facilitated by an enzymatic[10] or chemical[11] pre-treatment of the pulp fibers (Fig. 1a). Their high strength and stiffness (the modulus of the crystal exceeds 130 GPa along the *c*-axis[12]) make them interesting for a number of nanocomposite applications.[8,13] One major advantage of the thin, slender wood cellulose nanofibrils is their ability to entangle and form strong inter-fibril bonds facilitated by their hydroxyl-rich surfaces. This permits a variety of nanostructures with tunable porosity in the dry state; from strong and dense nanopapers[14] to porous ultra-light aerogels[15] and foams.[16] In addition, the hydroxyl groups present opportunities to actively participate in aqueous metal ion sol–gel reactions, where the nanofibril network in suspension serves to confine/interpenetrate metal solution complexes during the formation/condensation of nanoparticles.[3]

Here, we demonstrate a single-step method to prepare magnetic particle decorated, slender and flexible cellulose nanofibrils for colloidal suspensions that can be formed into strong and agglomeration-free nanocomposites with very high contents of the inorganic phase (>50 wt%). The method relies on the *in situ* precipitation of metal ions onto the nanofibrils (demonstrated to be nucleation sites) and the formation of a magnetic colloidal suspension or hydrogel, which can be liquid-processed into a flexible membrane – or shaped into any arbitrary geometry – by simple filtration or molding, and drying at room temperature. We also demonstrate how fibrils decorated with two different types of magnetic nanoparticles can be mixed in suspension to form composites with tunable and predictable magnetic properties. Finally, an ultra-thin loudspeaker prototype is demonstrated in which a coil directly drives a magnetic membrane without the need for any bulky external magnet. Bacteria-produced cellulose has previously been suggested as a replacement material within traditional headphones/earphones[17] due to its favorable mechanical properties (high specific toughness and dynamic strength, low density)[18] but without an integrated magnetic phase.
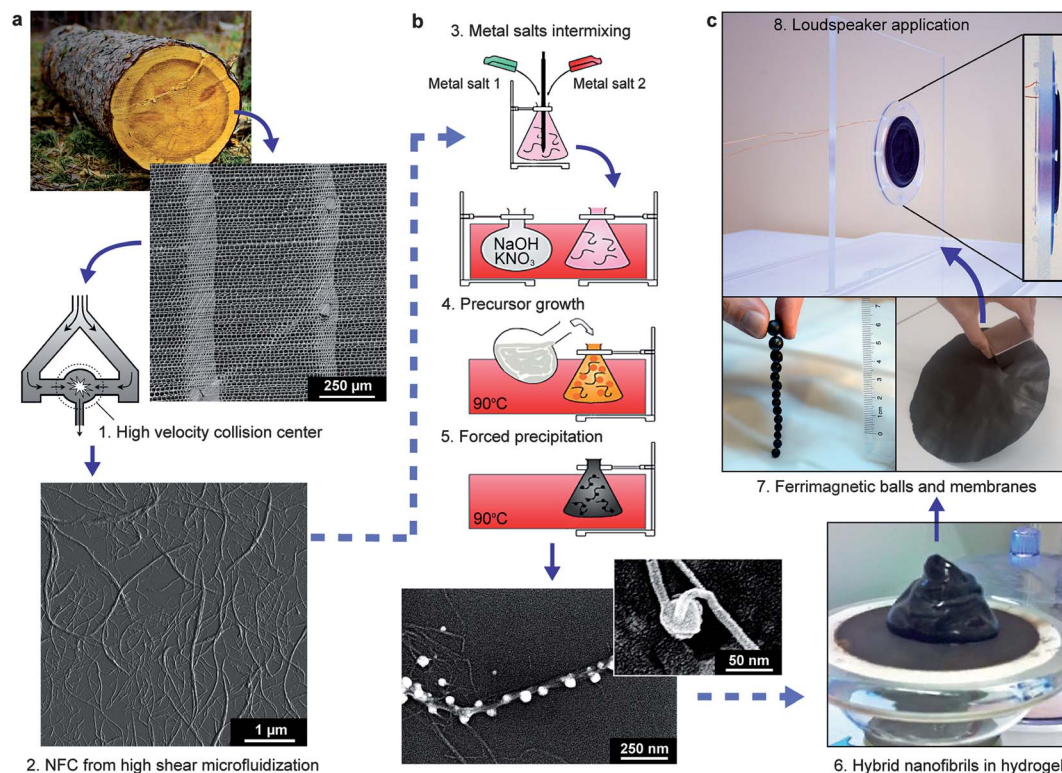

Fig. 1 Preparation of magnetic nanocomposites from decorated cellulose nanofibrils (NFC). (a) Structure of a softwood tissue; nanofibrils are extracted from the cell wall by high shear microfluidization; AFM image of the cellulose nanofibrils. (b) Magnetic ferrite nanoparticles are precipitated *in situ* onto nanofibrils from metal salt solutions; SEM image of a decorated nanofibril. (c) Formation of a magnetic hydrogel by water removal; further drying allows preparation of magnetic nanocomposites: hard permanently magnetized spherical beads were prepared by rotation of the hydrogel on a Teflon surface during drying overnight – large magnetic membranes (20 cm diameter) were prepared by vacuum filtration of the decorated nanofibril suspension; adaption of hybrid magnetic membranes in a thin prototype loudspeaker without external magnet. The numbers show the consecutive steps during the processing.

7964 | *J. Mater. Chem. C*, 2013, **1**, 7963–7972

This journal is © The Royal Society of Chemistry 2013

Results and discussion

Magnetic decoration of cellulose nanofibrils

The ferrite decorated cellulose nanofibrils were prepared by *in situ* precipitation of aqueous iron/cobalt (alt. iron/manganese) ion complexes onto cellulose I nanofibrils. The metal salts were mixed at room temperature with the suspended cellulose nanofibrils (liberated by enzymatic treatment and microfluidization) and heated to 90 °C at a rate of 2 °C min^{-1} before the rapid addition of the alkaline medium (Fig. 1b). The reaction permitted a complete metal ion condensation of the inorganic precursors as magnetic spinel ferrite crystals on the fibrils, which was confirmed by X-ray diffraction (ESI, Fig. S1†). The metal ion concentrations (from 3 to 45 mM) were approximated to yield hybrid fibrils with 10, 30 and 60 wt% nanoparticles (corresponding to 3, 10 and 21 vol%). Fig. 1b shows the morphology of the hybrid nanofibrils with magnetic particles grafted along the *c*-axis of the cellulose fibrils, occasionally embedding (surrounding) the nanofibrils. All the prepared samples showed a similar distribution of $CoFe_2O_4$ alt. $MnFe_2O_4$ particles along the fibril surfaces due to the heterogeneous nucleation and possibly uneven frequency of nucleation sites. The materials with the lowest relative particle contents (10 and 30 wt%) showed neat nanofibrils without particles, suggesting that the cellulose grafting sites (nucleation points) were in excess of the nucleating metal oxide, see further discussion under ESI, Table S1.† These unmodified fibrils were thinner and often significantly shorter than the bundled fibrils, possibly not providing stable nucleation sites similar to those on the bundled fibrils. The fraction of thin fibrils resulted from a greater enzymatic degradation of the non-crystalline wood components during the liberation of the nanofibrils from the pulp. Increasing the relative content of metal ions resulted in a smaller fraction of unmodified fibrils. The bonding of the particles appeared strong and black sediment or loose particles could not be separated from the fibril suspensions after extended periods of time (2 months), even on exposure to strong magnetic fields (a 20 cm^3 1.2 T magnet placed under the suspensions) and/or ultra-sonication at an estimated energy of 300 W during 2 min. The resistance against fragmentation indicated that the nanoparticles were firmly attached to the nanofibrils as a result of the presence of fibrils during particle formation. In rare cases, the crystallization of the particles seemed to take place in-between fibrils, merging them into a thicker fibril entity that encapsulates the magnetic nanoparticles, see ESI, Fig. S2.†

After synthesis, the *in situ* functionalized magnetic nanofibril suspensions had a solid content of 0.25 wt%, *i.e.* the combined cellulose and inorganic content. The minimum solid content for the hybrid fibril suspensions to display a single phase was 0.10–0.15 wt%, *i.e.* more dilute suspensions tended to separate due to gravity. At *ca.* 2 wt%, the suspension of magnetic fibrils behaved like a gel, retaining its shape in the wet state due to physical fibril entanglements (Fig. 1c and ESI, Video†). Upon vacuum filtration, the magnetic cellulose gel became a solid paste (*ca.* 50 wt% of water), which could be molded and processed into various shapes. The volume of the paste was reduced by an additional 75% on complete drying. The contraction of the material upon drying was measured from the diameter of small (5 mm) spheres that were prepared on a rotating table at room temperature (Fig. 1c). Other permanently magnetic nanocomposites were prepared from the solid paste *via* conventional drying, such as plates and membranes. Fig. 1c (top) shows the membrane mounted in a prototype loudspeaker actuated by a single external coil.

Phase interactions during forced hydrolysis synthesis

The presence of cellulose nanofibrils during the metal ion conversion resulted in smaller ferrite particles and a narrower particle size profile than when the particles were synthesized in the absence of fibrils (Fig. 2b). The particles grafted onto the fibrils were predominantly spherical in shape for all the *in situ* precipitated particle systems, in contrast to the cubic particles obtained when no cellulose was present during the synthesis (ESI, Fig. S3†). The ferrite particle shape has been described as related to the growth rate of the crystals; more rapid crystallization and growth yield less selective atom site condensation and spherical particles.[19] Here, the mixing rates and temperatures of chemicals were maintained the same during all the experiments, so that the particle shapes were expected to be the same. However, the randomly oriented cellulose nanofibrils in the suspensions not only functioned as a template in the metal ion sol–gel, but also affected the particle shape, possibly by confining or more evenly distributing the amount of metal species precipitated into each nanoparticle.[20] The average distance between adjacent fibrils in the prepared 0.3 wt% cellulose suspensions was *ca.* 200 nm, which is comparable to, or shorter than, the expected radius of metal hydroxide complexes developed during the heating of iron solutions, *i.e.* a few hundred nanometers.[21] In essence, the selected concentrations of cellulose fibrils were always sufficient to penetrate several times the metal ion complexes developed, in particular during the heating sequence. The heating of iron solutions enhances the formation of larger and more extended metal ion complexes and proceeds *via* oleation or oxolation reactions,[21,22] which is also shown as a conversion from transparent to translucent solutions. A key to proper particle attachment was to allow the hydroxyl functional groups on the cellulose fibrils to be in the proximity of the condensation and oxidation reactions of the metal ions, which in turn allowed 'directed' condensation of the metal ion sol–gel onto the fibril surfaces (Fig. 2c). Aliquots of the heated metal salt/ NFC solutions taken during the heating step (prior to the conversion of the precursors into the ferrite phase) confirmed this initial hypothesis and revealed the presence of solid acicular nanorods (a few nanometers in diameter and tens of nanometers long) firmly attached to the nanofibrils (Fig. 2c and 1b). The nanorods consisted of iron(III) oxo-hydroxides (XRD spectrum in ESI, Fig. S4†) and served as nucleation points for the magnetic ferrite phase. At this stage, the nanorods comprised only *ca.* 10 mol% of the total inorganic content in the 3 mM suspension and 2 mol% in the 45 mM suspension, *i.e.* 2–3 wt% of the total amount of hybrid cellulose nanofibrils. This relatively small but substantial amount was related to an initial very low metal ion
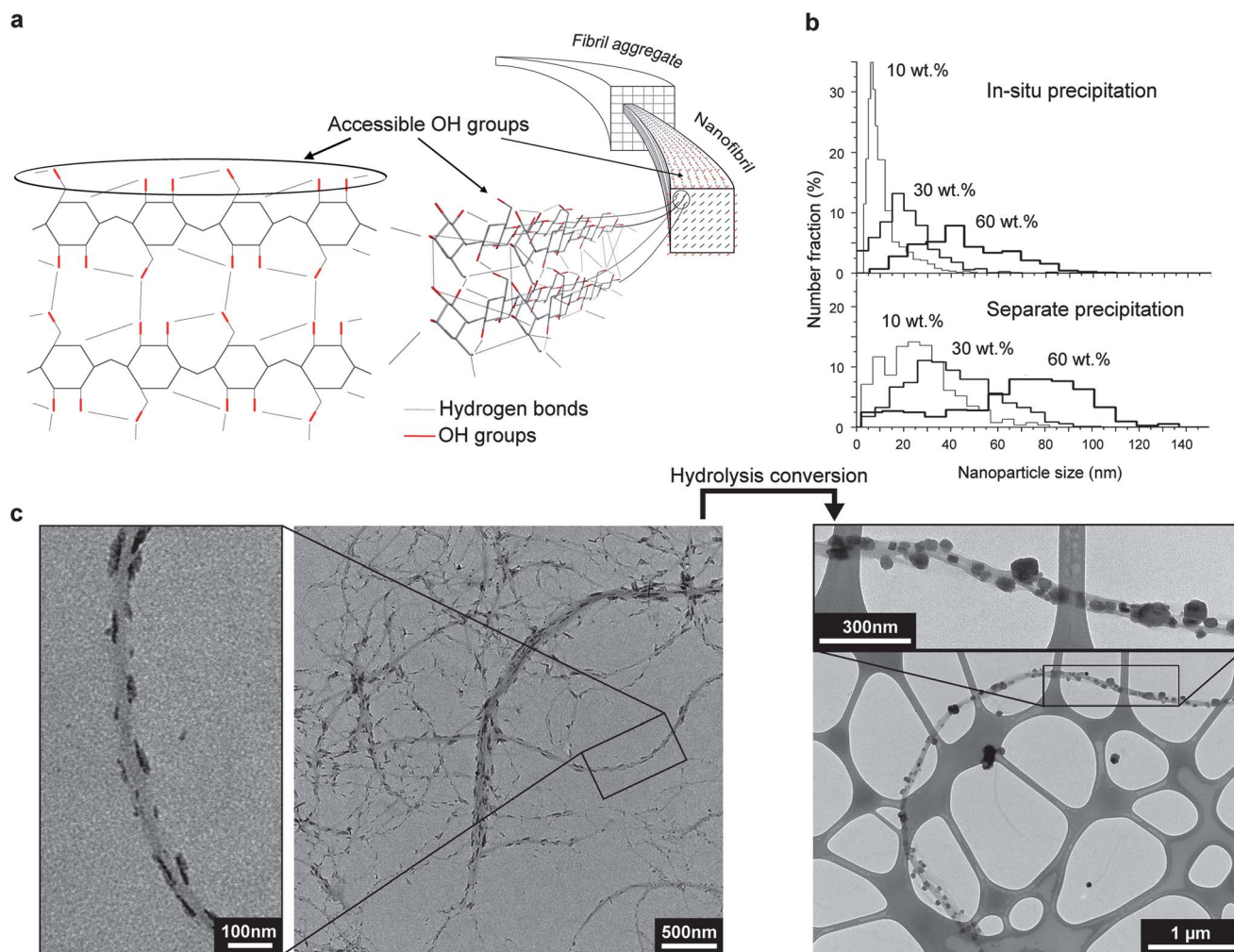
This journal is © The Royal Society of Chemistry 2013

J. Mater. Chem. C, 2013, **1**, 7963–7972 | **7965**

Fig. 2 Phase interactions during *in situ* precipitation. (a) Cellulose nanofibril structure showing accessible surface hydroxyl groups and intra-molecular hydrogen bonds. (b) Nanoparticle size distributions from TEM image analysis for particle precipitated in the presence ("*in situ*"), and in the absence ("separate") of cellulose nanofibrils. The wt% corresponds to the loading of the inorganic phase along the cellulose nanofibrils. (c) TEM images of the 30 wt% $CoFe_2O_4$ system, showing the precursor oxo-hydroxide rods on cellulose fibrils (representing *ca.* 1 wt% of the hybrid material, left side micrographs) from aliquot after heating the metal ion – cellulose suspension (Fig. 1b) prior to conversion into magnetic nanoparticles (right).

coverage of the theoretically accessible hydroxyl groups derived from the intrinsic structure of the cellulose nanofibrils (Fig. 2a). Induction-coupled plasma (ICP) spectroscopy revealed that only *ca.* 3% of the theoretical hydroxyl groups were occupied by metal ions prior to heating in the most dilute system, whereas the value increased to 15% in the 45 mM system (see ESI, Table S1†). The remainder of the non-occupied theoretically estimated OH-sites was thus hindered from adsorbing metal ions or were inaccessible due to strong hydrogen bonds with other hydroxyl groups in the cellulose crystals (Fig. 2a).[23] Belford *et al.*[24] reported similar numbers (10–20%) and suggested that metal ion adsorption on the outer surface of the nanofibrils is complete within 15 min at a metal ion concentration greater than 30 mM.

Formation of membranes from the magnetic hybrid fibrils

Large magnetic membranes (20 cm diameter) were prepared by vacuum filtration of the hybrid nanofibril suspensions

obtained by the *in situ* method. These membranes were compared with membranes obtained from separately precipitated particles mixed with suspensions of neat fibrils. Fig. 3 shows the dispersion of magnetic nanoparticles in the membranes prepared (a) *in situ* and (d) by mixing. The membranes prepared by high-shear mixing of the separate components showed a particle distribution significantly inferior to that in membranes prepared from the *in situ* functionalized fibrils. The particles were located as large aggregate pockets up to 2.5 μm in size, located between condensed bundles of cellulose nanofibrils, Fig. 3b (inset). Thus, the traditional mixing procedure allowed particles to associate and aggregate during the formation of the materials (due to magnetic dipolar and van der Waals interactions), as was simulated and observed by Lalatonne *et al.*[25] In contrast, the *in situ* precipitated particles were uniformly dispersed in the material due to their firm attachment and hindrance from associating during the water-removal process. The uniform
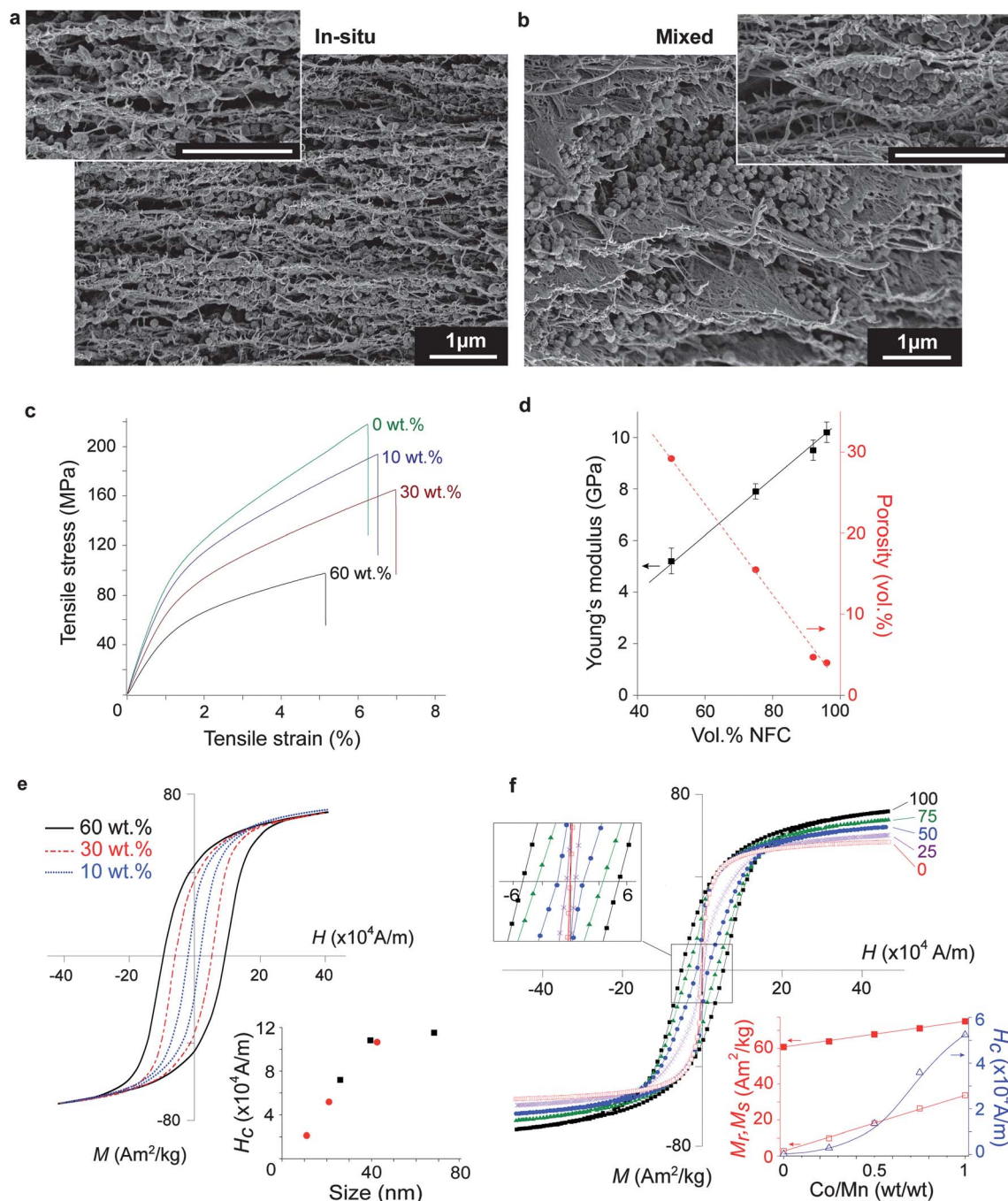
Fig. 3 Structure and properties of hybrid nanocomposite magnetic membranes, all scale bars 1 μm. (a) and (b), SEM micrographs of membranes: (a) 90° cross-sections showing homogeneous particle distribution from decorated nanofibrils. (b) 45° cross-sections with particle aggregation in micron sized pockets (inset – 90°) between inter-condensed fibrils from the mixing of the two separate compounds. (c) Stress–strain curves of magnetic membranes prepared from decorated nanofibrils. (d) Young's modulus and porosity as a function of volume fraction of cellulose nanofibrils. (e) Hysteresis loops for membranes made of nanofibrils decorated with different amount of CoFe$_2$O$_4$ nanoparticles; inset: the coercivity related to the size of nanoparticles (red circles: *in situ*, black squares: separate precipitation). (f) Hysteresis loops for membranes with different ratios of hybrid nanofibrils decorated with "hard" CoFe$_2$O$_4$ and "soft" MnFe$_2$O$_4$ nanoparticles from their suspensions – 100 refers to membranes obtained from solely CoFe$_2$O$_4$ functional fibrils, whereas 0 represents membranes composed solely of MnFe$_2$O$_4$ hybrid nanofibrils. Lower-right inset shows remanent, saturation magnetization and coercivity evolving with the material composition (experimental data points), and their accurate predictions (continuous lines).

distribution of particles can thus be traced back to the relatively uniform condensation of metal ion complexes along the fibrils, *i.e.* before the condensed metal ions were converted into the ferrimagnetic phase.

Membrane structure and mechanical properties

Data for the structural features and the mechanical properties are summarized in Table 1 and Fig. 3(c) and (d). The neat cellulose membranes showed an ultimate strength and Young's

This journal is © The Royal Society of Chemistry 2013

J. Mater. Chem. C, 2013, **1**, 7963–7972 | **7967**

Table 1 Characteristics of hybrid nanocomposite membranes (standard deviation in parenthesis)

Phase	Ferrite (wt/vol%)	ρ^a (g cm^{-3})	Pores (%)	E^b (GPa)	σ^c (MPa)	ε_r^d (%)	W_F^e (MJ m^{-3})	D_{NP}^f (nm)	M_r^g (A m^2 kg^{-1})	M_s^h (A m^2 kg^{-1})	H_c^i (kA m^{-1})
—	0/0	1.40	4.0	10.2 (0.4)	215 (8)	6.1 (0.4)	8.7 (0.5)	—	—	—	—
CoFe$_2$O$_4$	10.2/3.1	1.50	4.7	9.5 (0.4)	187 (6)	6.4 (0.3)	8.1 (0.4)	11	21.3	77.3	21.2
CoFe$_2$O$_4$	30.9/9.6	1.56	15.5	7.9 (0.3)	160 (5)	6.9 (0.3)	7.5 (0.3)	21	33.2	73.9	52.5
CoFe$_2$O$_4$	59.1/21.3	1.77	29.2	5.2 (0.5)	96 (9)	5.8 (0.4)	3.9 (0.4)	42	47.4	74.3	106.8
MnFe$_2$O$_4$	30.7/9.5	—	—	—	—	—	—	26	2.7	59.8	0.4

^{a} Density. ^{b} Young's modulus. ^{c} Ultimate tensile strength. ^{d} Tensile strain to failure. ^{e} Toughness, equivalent here to the work of fracture calculated from the area under the stress–strain curves (see Fig. 3c). ^{f} Number average nanoparticle diameter from size distributions of Fig. 2 (based on TEM analysis). ^{g} Remanent magnetization. ^{h} Saturation magnetization. ^{i} Coercivity.

modulus of 215 MPa and 10 GPa respectively. These values are comparable or superior to the currently strongest large-scale fabricated polymer membranes, e.g. biaxially oriented polyethylene terephthalate films (BO-PET/"Mylar"). In BO-PET, a high molecular orientation is obtained by stretching to give a tensile strength and stiffness in the range of 200–250 MPa and 4–8 GPa, respectively.[26] However, nanoparticle-filled films based on engineering polymers commonly show limited strength and stiffness (10–50 MPa, 1–2 GPa) at a relatively low particle content (<5 vol%) due to difficult processing and excessive nanoparticle aggregation.[7,27] In contrast, the present hybrid cellulose membranes with an inorganic content of 60 wt% (21 vol%) showed an ultimate strength of 100 MPa and a Young's modulus of 5 GPa (work of fracture: 3.9 MJ m^{-3}), which significantly exceed the previously reported values for polymer/nanoparticle composites, e.g. prepared by classical mixing of particles with polymers. Note the presence of a yield stress followed by a region of strain-hardening plastic deformation as the nanofibrils slide with respect to each other (Fig. 3d).[14] It is important to emphasize that it is the combination of strength, stiffness and ductility, e.g. toughness (work of fracture) that is the ultimate requirement for the design of dry magnetic nanocomposites, such as in the present membrane application. As a comparison, recently reported ultra-strong layer-by-layer assemblies of clay platelets/polymer nanocomposites show an impressive strength of 350 MPa,[28] but the extreme stiffness (106 GPa) in combination with limited ductility (0.3% strain to break) makes them impractical in many applications (work of fracture: 0.5 MJ m^{-3}). In contrast, previously reported wet magnetic polymer nanocomposites (hydrogels) show extensive deformation capacity and shape recovery,[29] but the ultimate strength and toughness of these materials deteriorate in the dry state and mechanical characteristics are therefore absent in the literature.

The explanation for the favorable mechanical properties of the cellulose membranes (besides the intrinsic structural features related to the cellulose crystals[12]) lies in the readily established nanofibrillar network throughout the material, which by its interpenetrating nature prevents early fracture due to localized failure events. The formation of the network relies not only on having cellulose nanofibrils with a high aspect ratio which promote extensive entanglements, but also readily accessible hydroxyl groups available to facilitate fibril interactions.[8,14] Nevertheless, the packing ability of the cellulose

nanofibrils into more dense membranes decreases with increasing inorganic content and physically larger particles, thereby limiting the number of nanofibril contacts. The resulting increase in network porosity (Table 1 and Fig. 3d) explains the observed linear decrease in strength and stiffness with increasing fractions of the particles (Fig. 3d). The decrease in Young's modulus can thus be estimated from the load-bearing NFC matrix alone (using the rule of mixtures), since the nanoparticles do not contribute to the macroscopic mechanical properties of the composites. Interestingly, these characteristics allowed for tuning the mechanical properties of the composites by modifying the nanofibril interactions. Here, different plasticizing molecules can favor or disrupt associative bonding between the fibrils simply by their presence in the network structure. As an example, water molecules acted as a plasticizer within the hybrid NFC network, showing on average 100% increase in strain-to-failure and only 10% reduction in strength as the conditions were varied from a completely dry to a saturated atmosphere (see ESI, Fig. S5†). The moisture content adsorbed during the conditioning of the membranes ranged, depending on inorganic content, from 10 wt% to 20 wt% after 2 weeks under humid conditions, which corresponds in all cases to ca. 30 vol% of the cellulosic matter. In this context, it should be stated that the composite membranes obtained from mixing particles and nanofibrils separately (Fig. 3d) resulted in similarly high mechanical strength values despite the presence of large aggregates (110 MPa strength at 60 wt%). A globally interconnecting nanofibril network thus tolerated particle aggregation without significantly disturbing the mechanical performance, which is in contrast to the behavior of traditional engineering polymer matrices. A similar behavior has previously been observed for clay nanopaper structures, which also show favorable mechanical properties at high inorganic contents.[30]

Tuning of the magnetic membrane properties

The intermixing of different hybrid fibrils functionalized with hard (CoFe$_2$O$_4$) and soft ferrite (MnFe$_2$O$_4$) nanoparticles (ESI, Fig. S2†) allowed tuning of the coercive magnetic properties of the membrane by two orders of magnitude with great accuracy, from 0.4 to 50 kA m^{-1}, see Fig. 3f. Here, two separate suspensions with separately decorated nanofibrils showed properties that closely followed a simple rule of mixing for the magnetic

moment (eqn (1)). The accuracy in the predicted magnetic behavior was ± 0.5–3% over the full hysteresis loops. The mixing could be performed by high-shear fluidization of the hybrid fibril suspensions, favoring the non-agglomerated state of particles within the final composites, due to the non-sedimenting magnetic phase. The hysteresis loops and magnetic data of the mixed composition membranes (normalized with respect to the nanoparticle mass) can be found in Fig. 3f and Table 2.

$$M_{comp}(H) = w_{soft} \, M_{soft}(H) + w_{hard} \, M_{hard}(H) \qquad (1)$$

where M_i is the magnetic moment, H is the applied field strength and w_i is the ferrite weight fraction.[31] The hysteresis curves for the membranes could thus be predicted from the pure cobalt and manganese ferrite components curves. ESI, Fig. S6† shows experimental data for the generated wasp-waist hysteresis loop at the 50–50 wt% composition, together with the predicted curve from eqn (1). Tuning the magnetic properties of the nanoparticles has in the past attracted significant attention and it has been accomplished by adjusting precipitation reactions to favor specific particle sizes or compositions. Efforts have covered a range of solution-based organic chemistry methods to obtain more predictable nucleation and growth with less size variability and more reproducible magnetic data.[32] However, the micro-emulsion or high-temperature batch reactions with limited yields are impractical for large-scale synthesis and rely on expensive environment-unfriendly chemicals. The traditional aqueous alternative has, in contrast, shown limited predictability due to the complexity of the reactions, including several phase transformations prior to the formation of the final particles.[33,34]

Table 1 and Fig. 3e show the magnetic data for the hybrid fibril components described in this study, which is in agreement with previous literature data for nano-sized ferrite nanoparticles.[35] In the case of the cobalt ferrite nanofibrils, a decreasing coercivity (Fig. 3e – inset) was recorded for smaller sized particles with more narrow size distributions (Fig. 2b), explained as related to an increasing fraction of particles below the superparamagnetic threshold (ca. 14 nm for $CoFe_2O_4$ (ref. 36)). A constant saturation magnetization was observed with the hybrid fibrils in spite of variations in the particle size. Overall, the presence of nanofibrils during synthesis (reducing the average particle size by ca. 50%) affected the magnetic properties in a manner that could be expected from the smaller sized particles,

i.e. the coercivity values were smaller than those with the larger particles formed 'separately' from the same salt concentrations, Fig. 3e. Notably, the regular hysteresis shape and size-dependence suggest that the particles were essentially non-interacting; which was further supported by the strictly additive properties obtained on the mixing of hard and soft magnetic nanofibrils. This indicates that exchange coupling between the two kinds of nanoparticles,[37] which requires the particles to come within a few atomic distances from each other, was absent.

Application of the membranes in a novel loudspeaker design

The combination of magnetic and mechanical functionality of the membrane enabled the construction of a novel super-thin loudspeaker prototype (Fig. 4). Traditional loudspeakers have a voice coil bonded to a geometrically shaped acoustic membrane, which is suspended in the magnetic field of a bulky permanent magnet. Mechanical forces act on the coil with an applied current, allowing the formation of pressure gradients as the coil and membrane are moved in the air. In contrast, the presented prototype makes the external magnet unnecessary because it constitutes an integral part of the acoustically active membrane, while the coil (carrying the signal current) driving the membrane is being kept stationary to eliminate any moving electrical parts. This design was possible due to the advantageous mechanical (high stiffness and strength) and ferrimagnetic properties of the magnetic nanofibrillar membrane. The evaluated prototype was realized using the 60 wt% ferrite-loaded membrane mounted in a poly(methyl-methacrylate) baffle plate (Fig. 1c and 4a), with a thin copper coil (75 mm inner diameter) leveled in line with the membrane (Fig. 4a and b). The sound output of the speaker prototype was of good quality (recording of a song by Romi Mayes played on the loudspeaker is available as ESI Audio file†), also illustrated by the reasonably flat frequency response (especially in the audible range from 20 Hz to 15 kHz, Fig. 4c). Since the force applied to the membrane is proportional to the membrane's remanent magnetic moment and to the magnetic field gradient (Fig. 4b), the design can be further improved to favor higher sound pressure levels by optimizing the geometrics, or by increasing the magnetic moment inside the membrane (e.g. higher loading of nanoparticles). Implementation of this concept of loudspeaker can possibly compete with other technologies in the design of large flat, ultrathin speakers[38] or as compact and lightweight miniature speakers for specific purposes (hearing aids, transducers and noise cancellation technologies).

Conclusions

Cellulose nanofibers from wood have been decorated by ferrite nanoparticles in an *in situ* process so that the magnetic ferrite nanoparticles are well dispersed and distributed along the nanofibers. This was carried out in a single-step process by introducing cellulose nanofibrils when the nanoparticles are formed. The nanoparticles firmly attach to the nanofibrils by strong interactions and present a robust functionalized nano-building block. These hybrid nanofibrils can be flow-processed as a regular hydrocolloidal liquid system, and offer a range of

Table 2 Measured and predicted magnetic properties of mixed hard/soft nanocomposites (measured/predicted)

Co/Mn[a] (wt%)	M_r[b] (A m² kg⁻¹)	M_s[c] (A m² kg⁻¹)	H_c[d] (kA m⁻¹)
100/0	33.2	73.9	52.5
75/25	26.0/25.6	70.0/70.4	36.0/34.1
50/50	17.9/18.0	66.7/66.9	14.0/11.2
25/75	9.7/10.3	62.9/63.3	3.1/2.9
0/100	2.7	59.8	0.4

[a] Proportions of nanofibrils with hard $CoFe_2O_4$ and soft $MnFe_2O_4$. [b] Remanent magnetization. [c] Saturation magnetization. [d] Coercivity.
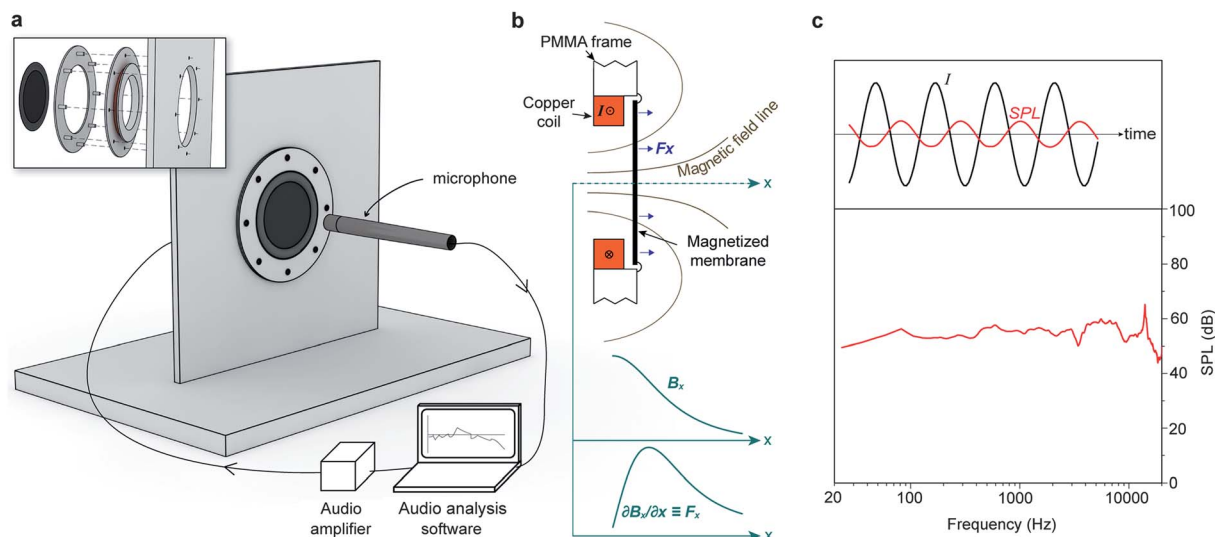
Fig. 4 Magnetic nanocomposite membrane in the prototype loudspeaker. (a) Scheme of the recording setup for the acoustic measurements in the anechoic chamber – the membrane was 50 μm thick with 60 wt% $CoFe_2O_4$ nanoparticles and magnetized along the thickness direction using a 1.2 T NdFeB magnet. (b) Illustration of the working principle for the loudspeaker – the copper coil generates a magnetic field gradient exerting a force on the magnetized membrane; and the electric signal is reproduced as an acoustic vibration of the membrane, *i.e.* audible sound. (c) Frequency response of the loudspeaker recorded for 1 W active input power; the top shows, qualitatively, the non-deformed acoustic signal (red) recorded for a mono-frequency input current (black). A recording of of a song by Romi Mayes played on the loudspeaker is available as ESI Audio file.†

opportunities for nanocomposite preparation, *e.g.* functional reinforcement, complex shape molding, coating, templating, *etc.* giving specific advantages over conventional approaches where preformed nanoparticles are mixed with engineering polymers. In suspension, the decorated nanofibrils were stable (>0.2 wt%) and formed a solid magnetic gel at contents >2 wt%. Upon drying, the coalescence of decorated nanofibrils into an interpenetrating network ensured uniform and agglomeration-free nanoparticle distribution in the final nanocomposite, with preserved mechanical properties at a high inorganic content (100 MPa strength, 5 GPa stiffness at 60 wt% $CoFe_2O_4$) and adjustable as well as predictable magnetic properties. The potential of this combination of liquid-processing, mechanical and magnetic properties was demonstrated in a very thin prototype loudspeaker where the membrane was directly driven to generate music by a single static coil. The membranes can be envisioned in small loudspeakers, hearing aids, noise reduction technologies, *etc.* where stiffness, strength and toughness are required. Additionally, the inexpensive character and low environmental impact of this approach make it interesting for large-scale development. The "*in situ*" precipitation methodology could be extended to other metal oxide nanoparticle systems, providing new opportunities in applications where functionalities of high surface area nanoparticles at relatively large weight fractions need to be combined with a strong and tough nanostructured network.

Experimental

In situ precipitation of magnetic ferrite nanoparticles on cellulose nanofibrils

Cellulose nanofibrils were extracted from commercial wood pulp according to Henriksson *et al.*[10] utilizing an enzymatic pre-treatment procedure followed by high shear micro-fluidization, see ESI Methods.† Reagent grade iron(II) sulphate heptahydrate and cobalt(II) or manganese(II) chloride hexahydrate, were added to a 1.2 L suspension of cellulose nanofibrils (0.3 wt% dry contents) under high-shear mixing (Ultra Turrax Di25) to ensure a uniform suspension. The stoichiometric ratio of cobalt or manganese to iron was 1 : 2. Sodium hydroxide and potassium nitrate (reagent grade) were dissolved in 0.4 L of distilled water. The solutions were heated separately to 90 °C under mechanical stirring (200 rpm), and the alkaline solution was quickly (3 s) added to the metal-ion-cellulose suspension under intense mechanical stirring (500 rpm). The co-precipitation reactions were performed with different amounts of metal salts in order to vary the nanoparticle content on the hybrid cellulose nanofibrils. The target amounts were 10 wt%, 30 wt% and 60 wt% nominal loading of the inorganic phase along the fibrils, corresponding to 3, 12 and 45 mM of metal salts dissolved in the fibril suspensions. The $[Me^{2+}]/[OH^-]$ and $[Me^{2+}]/[KNO_3]$ ratios were kept constant and equal to 1/2 and 1/3, respectively, according to Olsson *et al.*[3,34] The reaction time was 6 h at 90 °C to ensure complete conversion of the metal oxide-hydroxide complexes/precursors into the spinel ferrite phase on the cellulose nanofibrils.[34] The modified fibrils were rinsed and cleaned from the metal salt counter-ions with distilled water at least 4 times by centrifugation.

Separate preparation of ferrite nanoparticles for mixing with cellulose nanofibrils

Manganese and cobalt ferrite nanoparticles were synthesized under exactly the same reaction conditions as above but in the absence of cellulose. The specifics of the aqueous co-precipitation of the ferrite nanoparticles were described in a previous

7970 | *J. Mater. Chem. C*, 2013, **1**, 7963–7972

This journal is © The Royal Society of Chemistry 2013

article.[34] The yields of these reactions were determined gravimetrically after oven-drying of 5 mL aliquot samples at 105 °C for 24 h. The separately prepared nanoparticle suspensions were then mixed with the different amounts of NFC to prepare membranes with the same fractions of nanoparticles as in the case of the *in situ* modified nanofibrils (10, 30 and 60 wt% inorganic phase).

Preparation of magnetic nanocomposite membranes

Large magnetic cellulose membranes (20 cm diameter, 50–70 μm thick) were made from the "*in situ*" decorated cellulose nanofibrils by vacuum filtration and further drying in a vacuum oven at 93 °C.[39] All the membranes prepared according to the above scheme are referred to as "*in situ*" to emphasize that the particles were precipitated directly onto the cellulose fibrils. The membranes obtained solely by mixing nanofibrils and nanoparticles are referred to as "*separate/mixed*" to emphasize that the components were prepared separately.

Metal adsorption study and precursor quantification

Two separate 30 mL aqueous cellulose nanofibril suspensions (0.1 g of cellulose nanofibrils, *i.e.* 0.3% dry content) with metal salt concentrations corresponding to the 10 and 60 wt% systems (*i.e.* molarities of 3 and 45 mM) were continuously stirred for 1 h to quantify the absorption of metal ions onto the cellulose fibrils. After rinsing several times with deionized water, the amount of metal cations adsorbed was measured by Induction Coupled Plasma - Optical Emission Spectroscopy (ICP-OES). The same procedure was used but with continuous heating at 90 °C in order to determine the amount of metal precipitated into the oxo-hydroxide precursors. The calculation of the theoretical numbers of adsorption sites on the cellulose fibrils is explained in the ESI (discussion of Table S1†).

Characterization of decorated nanofibrils and magnetic hybrid nanocomposite membranes

Scanning (SEM) and transmission (TEM) electron microscopy were used to characterize the prepared suspensions of decorated nanofibrils. The sample preparation is described in ESI Methods.† SEM was used for general hybrid nanofibril characterization, whereas TEM was used for nanoparticle size distribution measurements. Mechanical testing was carried out on strips (5 mm width/50 μm thickness) from the prepared membranes, which were tested in tension in a controlled climate (23 °C, 50 %RH). Samples were preconditioned below 5 %RH and above 95 %RH to study the relationship between the mechanical properties and the membranes' moisture sensitivity. The hysteresis magnetization curves were recorded using a Vibrating Sample Magnetometer (VSM). The inorganic phase in the dry membranes was characterized by X-ray diffraction (ESI†). The total inorganic content in the prepared hybrid nanocomposite membranes was determined by thermo-gravimetric analysis (TGA) (ESI, Fig. S7†). More details of the above procedures can be found in the ESI Methods.†

Acoustic measurements

The super thin prototype loudspeaker based on the membranes derived from the "*in situ*" functionalized hybrid fibrils was tested in a full anechoic chamber with a transparent floor-grid. 50 μm thick membranes with 60 wt% cobalt ferrite nanoparticle loading were evaluated as mounted in a circular rotary cut in a 5 mm thick poly(methyl-methacrylate) baffle plate (300 × 300 mm), see Fig. 4. A coil support edge (also PMMA) surrounding the 75 mm circular cut (glued onto the baffle plate) contained 180 turns of insulated copper wire (0.5 mm). The resistance of the coil was accurately determined using a 4-probe technique, and the inductance was determined from the resonance frequency (3.560 kHz) of the coil combined with a precision capacitor, 1.001 μF ± 0.1%. The membranes were magnetized in the thickness direction using a 1.2 T NdFeB magnet (5 × 5 × 2 cm^3) prior to mounting. Output sound was recorded with an ICP MA201 microphone (Scantek Inc, USA) placed at a distance of 5 cm from the membrane. The input voltage was set to 17 V_{RMS}, and the measurements of output sound pressure were normalized to 1 W input active power (calculated from the voltage using measured values of the coil's inductance: 2.00 mH and resistance: 2.80 Ω).

Notes and references

1 S. Weiner and H. A. Lowenstam, *On biomineralization*, Oxford University Press, 1989.

2 Y. Dzenis, *Science*, 2008, **319**, 419.

3 R. T. Olsson, M. A. S. A. Samir, G. Salazar-Alvarez, L. Belova, V. Ström, L. A. Berglund, O. Ikkala, J. Nogues and U. W. Gedde, *Nat. Nanotechnol.*, 2010, **5**, 584.

4 S. Behrens, *Nanoscale*, 2011, **3**, 877.

5 Q. Dai and A. Nelson, *Chem. Soc. Rev.*, 2010, **39**, 4057; T. Hoare, J. Santamaria, G. F. Goya, S. Irusta, D. Lin, S. Lau, R. Padera, R. Langer and D. S. Kohane, *Nano Lett.*, 2009, **9**, 3651; A. C. Balazs, T. Emrick and T. P. Russell, *Science*, 2006, **314**, 1107; B. A. Evans, L. F. Fiser, W. J. Prins, D. J. Rapp, A. R. Shields and D. R. Glass, *J. Magn. Magn. Mater.*, 2012, **324**, 501.

6 M. E. Mackay, A. Tuteja, P. M. Duxbury, C. J. Hawker, B. Van Horn, Z. Guan, G. Chen and R. S. Krishnan, *Science*, 2006, **311**, 1740; R. Fuhrer, E. K. Athanassiou, N. A. Luechinger and W. J. Stark, *Small*, 2009, **5**, 383.

7 R. T. Olsson, M. S. Hedenqvist, V. Ström, J. Deng, S. J. Savage and U. W. Gedde, *Polym. Eng. Sci.*, 2011, **51**, 862; R. Fuhrer, C. M. Schumacher, M. Zeltner and W. J. Stark, *Adv. Funct. Mater.*, 2013, **23**, 3845.

8 S. J. Eichhorn, A. Dufresne, M. Aranguren, N. E. Marcovich, J. R. Capadona, S. J. Rowan, C. Weder, W. Thielemans, M. Roman, S. Renneckar, W. Gindl, S. Veigel, J. Keckes, H. Yano, K. Abe, M. Nogi, A. N. Nakagaito, A. Mangalam,

This journal is © The Royal Society of Chemistry 2013

J. Mater. Chem. C, 2013, **1**, 7963–7972 | 7971

J. Simonsen, A. S. Benight, A. Bismarck, L. A. Berglund and T. Peijs, *J. Mater. Sci.*, 2009, **45**, 1.

9 A. F. Turbak, F. W. Snyder and K. R. Sandberg, *J. Appl. Polym. Sci.: Appl. Polym. Symp.*, 1983, **37**, 815.

10 M. Henriksson, G. Henriksson, L. A. Berglund and T. Lindström, *Eur. Polym. J.*, 2007, **43**, 3434.

11 T. Saito, S. Kimura, Y. Nishiyama and A. Isogai, *Biomacromolecules*, 2007, **8**, 2485.

12 I. Sakurada, Y. Nukushina and T. Ito, *J. Polym. Sci.*, 1962, **57**, 651.

13 A. Walther, J. V. I. Timonen, I. Díez, A. Laukkanen and O. Ikkala, *Adv. Mater.*, 2011, **23**, 2924.

14 M. Henriksson, L. A. Berglund, P. Isaksson, T. Lindström and T. Nishino, *Biomacromolecules*, 2008, **9**, 1579.

15 M. Paakko, J. Vapaavuori, R. Silvennoinen, H. Kosonen, M. Ankerfors, T. Lindstrom, L. A. Berglund and O. Ikkala, *Soft Matter*, 2008, **4**, 2492; H. Sehaqui, Q. Zhou and L. A. Berglund, *Compos. Sci. Technol.*, 2011, **71**, 1593.

16 A. J. Svagan, M. A. S. A. Samir and L. A. Berglund, *Adv. Mater.*, 2008, **20**, 1263.

17 M. Uryu and N. Kurihara, *U.S. Pat., 5,274,199*, 1993.

18 Y. Nishi, M. Uryu, S. Yamanaka, K. Watanabe, N. Kitamura, M. Iguchi and S. Mitsuhashi, *J. Mater. Sci.*, 1990, **25**, 2997.

19 Q. Song and Z. J. Zhang, *J. Am. Chem. Soc.*, 2004, **126**, 6164.

20 F. Schüth, *Angew. Chem., Int. Ed.*, 2003, **42**, 3604.

21 M. Schultz, W. Burckhardt and S. Barth, *J. Mater. Sci.*, 1999, **34**, 2217.

22 C. F. Baes and R. E. Mesmer, *The hydrolysis of cations*, Wiley, 1976; J. P. Jolivet, M. Henry and J. Livage, *Metal oxide chemistry and synthesis: from solution to solid state*, John Wiley, 2000.

23 Y. Nishiyama, P. Langan and H. Chanzy, *J. Am. Chem. Soc.*, 2002, **124**, 9074.

24 D. S. Belford, A. Myers and R. D. Preston, *Biochim. Biophys. Acta*, 1959, **34**, 47.

25 Y. Lalatonne, J. Richardi and M. P. Pileni, *Nat. Mater.*, 2004, **3**, 121.

26 W. A. MacDonald, *J. Mater. Chem.*, 2004, **14**, 4.

27 S. M. Liff, N. Kumar and G. H. McKinley, *Nat. Mater.*, 2007, **6**, 76.

28 P. Podsiadlo, A. K. Kaushik, E. M. Arruda, A. M. Waas, B. S. Shim, J. Xu, H. Nandivada, B. G. Pumplin, J. Lahann, A. Ramamoorthy and N. A. Kotov, *Science*, 2007, **318**, 80.

29 Y. Li, G. Huang, X. Zhang, B. Li, Y. Chen, T. Lu, T. J. Lu and F. Xu, *Adv. Funct. Mater.*, 2013, **23**, 660.

30 A. Liu and L. A. Berglund, *Carbohydr. Polym.*, 2012, **87**, 53.

31 A. P. Roberts, Y. Cui and K. L. Verosub, *J. Geophys. Res.: Space Phys.*, 1995, **100**, 17909.

32 Y. Lee, J. Lee, C. J. Bae, J. G. Park, H. J. Noh, J. H. Park and T. Hyeon, *Adv. Funct. Mater.*, 2005, **15**, 503; S. Gyergyek, D. Makovec, A. Kodre, I. Arčon, M. Jagodič and M. Drofenik, *J. Nanopart. Res.*, 2010, **12**, 1263.

33 J.-P. Jolivet, C. Chaneac and E. Tronc, *Chem. Commun.*, 2004, 481; G. Salazar-Alvarez, R. T. Olsson, J. Sort, W. A. A. Macedo, J. D. Ardisson, M. D. Baró, U. W. Gedde and J. Nogués, *Chem. Mater.*, 2007, **19**, 4957.

34 R. T. Olsson, G. Salazar-Alvarez, M. S. Hedenqvist, U. W. Gedde, F. Lindberg and S. J. Savage, *Chem. Mater.*, 2005, **17**, 5109.

35 X.-H. Li, C.-L. Xu, X.-H. Han, L. Qiao, T. Wang and F.-S. Li, *Nanoscale Res. Lett.*, 2010, **5**, 1039.

36 T. Sato, T. Iijima, M. Seki and N. Inagaki, *J. Magn. Magn. Mater.*, 1987, **65**, 252.

37 L. H. Bennett and E. Della Torre, *J. Appl. Phys.*, 2005, **97**, 10E502.

38 L. Xiao, Z. Chen, C. Feng, L. Liu, Z.-Q. Bai, Y. Wang, L. Qian, Y. Zhang, Q. Li, K. Jiang and S. Fan, *Nano Lett.*, 2008, **8**, 4539; J.-H. Kim, S. Yun, J.-H. Kim and J. Kim, *J. Bionic Eng.*, 2009, **6**, 18.

39 H. Sehaqui, A. Liu, Q. Zhou and L. A. Berglund, *Biomacromolecules*, 2010, **11**, 2195.

This journal is © The Royal Society of Chemistry 2013